BAJOPAS Volume 15 Number 2, December, 2022

http://dx.doi.org/10.4314/bajopas.v15i2.7

Bayero Journal of Pure and Applied Sciences, 15(2): 41 - 48
Received: 8th July, 2022
Accepted: 21st Sept., 2022
ISSN 2006 – 6996

POLYPYRROLE/ Zn-doped TiO_2 NANOCOMPOSITE FOR CORROSION CONTROL OF MILD STEEL IN 3.5% NaCl SOLUTION

Ladan, M.,[1*] Tahir, R. U.,[1] Idris, M. B.,[2] Habibu, S.[2] and Salis, A. A.[1]
[1] Department of Pure and Industrial Chemistry, Bayero University Kano P.M.B. 3011, Kano Nigeria
[2] Department of Chemistry, Federal University Dutse, P.M.B 7156, Jigawa State Nigeria
Corresponding author: mladan.chm@buk.edu.ng

ABSTRACT
In recent years conducting polymers (CPs) have been paid more attention as new materials for several applications. Among the various uses of CPs corrosion protection of metals has attracted the attention of many researchers. Herein, we report the synthesis and corrosion protection activity of polypyrrole and polypyrrole/ Zn-doped TiO_2 nanocomposites. Scanning electron microscopy revealed a spherical shape of the PPy. The XRD and EDX results confirmed the presence of nanoparticles in the nanocomposite. The corrosion performance of the coatings on mild steel was evaluated by corrosion current measurement in 3.5 % NaCl solution. From the corrosion current measurement using hamfield corrosion studies kit, the corrosion rate of the coating was found to be 0.156 mm/yr and 75.51 % protection efficiency after 8 days. This is likely due to the increased surface area of the PPy synthesized in the presence of the Zn/TiO_2 NPs. It is evident that the presence of Zn/TiO_2 NPs can enhance the resistance against corrosion at the steel/electrolyte interface.

INTRODUCTION

Corrosion of materials such as mild steel causes big losses in the economy of many countries due to the huge amount of funds needed in order to minimize it. For instance, previous studies have estimated that the cost of corrosion in the USA alone stands at 276 billion each year represent 3.1 % of the US gross domestic product (GDP) (Thompson *et al.*, 2007 and Hsieh *et al.*, 2013). Thus research on corrosion protection and mitigation are important long term investments due to the economic and environmental concerns (Wei *et al.*, 2015). Despite the existence of many corrosion prevention techniques, it is still important to develop new approaches to decrease the effect of corrosion.

Conducting polymers (CPs) are quite promising for use as corrosion resistance agents to protective coatings (Lei *et al.*, 2015 and Bai *et al.*, 2015). Among the conducting polymers, polypyrrol (PPy) and polyaniline (PANI) have been examined as corrosion resistance coatings for diverse metal substrates, including steel, aluminium and copper (Yuan *et al.,* 2016 and Kamaraj *et al.*, 2010). Electro-active polymer-based inorganic nanocomposites also have been given some consideration based on their excellent physical properties in the development of corrosion protection of metals (Singh *et al.,* 2013 and Deyab and Keera, 2014). In recent years, polypyrrole based nanocomposites are the most utilized due to their high stability, environmentally benign and facile preparation in aqueous media (Mahmoudian *et al.*, 2013). The polymers prepared in the vicinity of nanoparticles have increased surface area (Lenz et al., 2003). This increases their capability of interaction with the released ions in the process of corrosion. Recent studies on polypyrrole/TiO_2 NCs as corrosion coating have shown that charge transfer resistance of coating can be improved by the presence of TiO_2. The anticorrosive properties of polypyrrole nanocomposite coating on steel is a result of the formation of stable passive oxide layers such as α-Fe_3O_4, α-Fe_2O_3 and β-Fe_2O_3 at the polymer-metal interface (Lenz et al 2003). Ladan *et al.*, (2017) synthesized a polypyrrole nanocomposites in the presence of TiO_2 and co-doped TiO_2 nanoparticles by in situ chemical oxidative polymerization in the presence of methyl orange as a soft template. The samples were characterized by FE- SEM, FTIR, XRD, TEM and TGA. The performance of the samples against corrosion were evaluated by incorporating the polymer samples in a butvar coating and tested on steel, the protection efficiency of the PPy/TiO_2 and co-doped TiO_2/PPy samples were evaluated after 30 days of exposure of the coated steel samples in 3.5% NaCl solution.

The result from electrochemical impedence spectroscophy (EIS) and potentiodynamic measurements showed that presence of co-doped TiO_2 NPs in the coating enhances the resistance against corrosion at the steel-electrolyte interface. In another study by Mahmoudian et al., (2011). They synthesizes PPy/Sn-doped TiO_2 nanocomposite and reported that the doping of Sn in TiO_2 lattice increases the anti-corrosion performance of the polymer coating.

In the present studies, polypyrrole and polypyrrole/ Zn-doped TiO_2 nanocomposites were synthesised, characterized, and evaluated for corrosion protection.

EXPERIMENTAL SECTION

MATERIALS

Pyrrole and titanium tetraisopropoxide were purchased from Sigma Aldrich whereas Iron (iii) Chloride and acetic acid were purchased from BDH.

Synthesis of Zn/ TiO_2 and TiO_2 nanoparticles

The Zn/TiO_2 NPs was prepared by sol-gel technique using titanium tetra isopropoxide ($Ti[OCH(CH_3)_2)]_4$ and zinc acetate as the precursors. At the beginning, the titanium precursor and zinc acetate were mixed with glacial acetic acid, with double distilled water added into the mixture. The molar ratio of the Zn-doped TiO_2 (3 mol %) nanocomposite was 1: 10: 200 for $(Ti[OCH(CH_3)_2)]_4$: glacial acetic acid : H_2O respectively. The solution was stirred constantly for 6 hrs and kept for 24 hrs at an ambient temperature to form a gel. The as-synthesized gel was placed at 75 ˚C in an oven, after which the obtained particles were ground to fine powders and finally calcined at 500 ˚C for 5 hrs. The TiO_2 NPs were also prepared using the same procedures for comparison with the Zn/ TiO2.
NPs (Mugundan et al., 2015)

Preparation and characterization of Zn doped TiO_2/PPy nanocomposites

For the preparation of polypyrrole doped Zn/TiO_2nanocomposite, 5.4 g $FeCl_3$ was added to 100 mL of water. The uniform solution was resulted by using magnetic mixer. After 30 minutes 0.24 g of Zn/TiO_2 NPs was added to the solution and after 20 min 1 mL fresh pyrrole monomer was added to the stirred solution. The reaction was carried out for 6 hrs at room temperature. Consequently, the product was filtered to separate the impurities, product was washed several times with de-ionized water and dried at 60 ˚C in oven for 24 hrs (Al-sabagh et al., 2016).

Physicochemical characterizations

X-ray diffraction (XRD) was performed to confirm the presence of TiO_2 and Zn/TiO_2 NPs in the PPy matrix and to determine the size of the nanoparticles. The morphology of the Zn/TiO_2/PPy, TiO_2/PPy and PPy were characterized by SEM Pw 100-002 microscope (Phenon proxy,). The chemical bonding of the nanocomposites was analyzed with FT-IR spectrophotometer 84003 (Shimadzu). The differential scanning calorimetry analysis (DSC) was performed to measure the thermal stabilities of the PPy, TiO_2/PPy NCs, and Zn-doped TiO_2 /PPy NCs respectively, at a heating rate of 10 ˚C/min under nitrogen atmosphere. The elemental analysis of the samples (EDX) were carried out using (Phenon proxy, model no, Pw 100-002) in the same manner as SEM.

Coating formulations of Zn-doped TiO_2/PPy NCs for corrosion tests

0.2 g of PPy/Zn/TiO_2 nanocomposite was dispersed in 12 ml of clear epoxy with continuous stirring for 20 hrs. Afterward, 8 ml of hardener was then added to the above solution under stirring for another 4 hrs at 400 rpm, thus yielding a black viscous solution with uniformly dispersed Ppy/Zn/TiO_2 nanocomposite and without settling (Xinxin Sheng et al., 2016). For comparison PPy and PPy/TiO_2 coatings were also prepared by similar method. Iron coupons (mild steel) 2 cm × 3 cm × 0.2 cm were mechanically polished with emery paper of different grades followed by rinsing with acetone and distilled water before coating and corrosion experiment. (Olad et al., 2010).

Dip coating technique

The already prepared mild steel samples were dip-coated for 30 s in a PPy/Zn-doped TiO_2 NCs epoxy coating solution and dried at ambient temperature for 20 min. The coated steel samples were then air dried at 50 ˚C in an oven for 24 hrs. Steel panels coated with epoxy incorporated with TiO2/PPy NCs and PPy were also prepared, and a steel panel coated with epoxy alone was used as the control. The steel samples with a coating thickness of 80 μm were used for the corrosion tests.

Fig. 1. Corrosion studies kit showing the metal samples in 3.5 % NaCl

Corrosion current measurement using corrosion studies kit

The rate of corrosion (corrosion current) of the coated and uncoated steel samples was measured using Armfield corrosion test kit in 3.5% NaCl solution. The already prepared NaCl solution was divided into different containers in which the samples were kept. The electrometer was then connected in series to each of the sample setup. The setup was then kept in that condition for another one week and the corrosion current was noted daily. After the seven days, the corrosion rate was then calculated using equation (1).

$$Corrosion\ rate\ (mm/yr) = k_1 * I_{corr} * \frac{EW}{\rho} \text{.....(1)}$$

Where, k_1; constant = $3.27*10^{-3}$ mm g/µA cm yr, I corr = current density in micro ampere per centimeter square (µA. cm^{-2}), EW = equivalent weight of metal, ρ = density of metal.

RESULTS AND DISCUSSION

Physicochemical Characterization

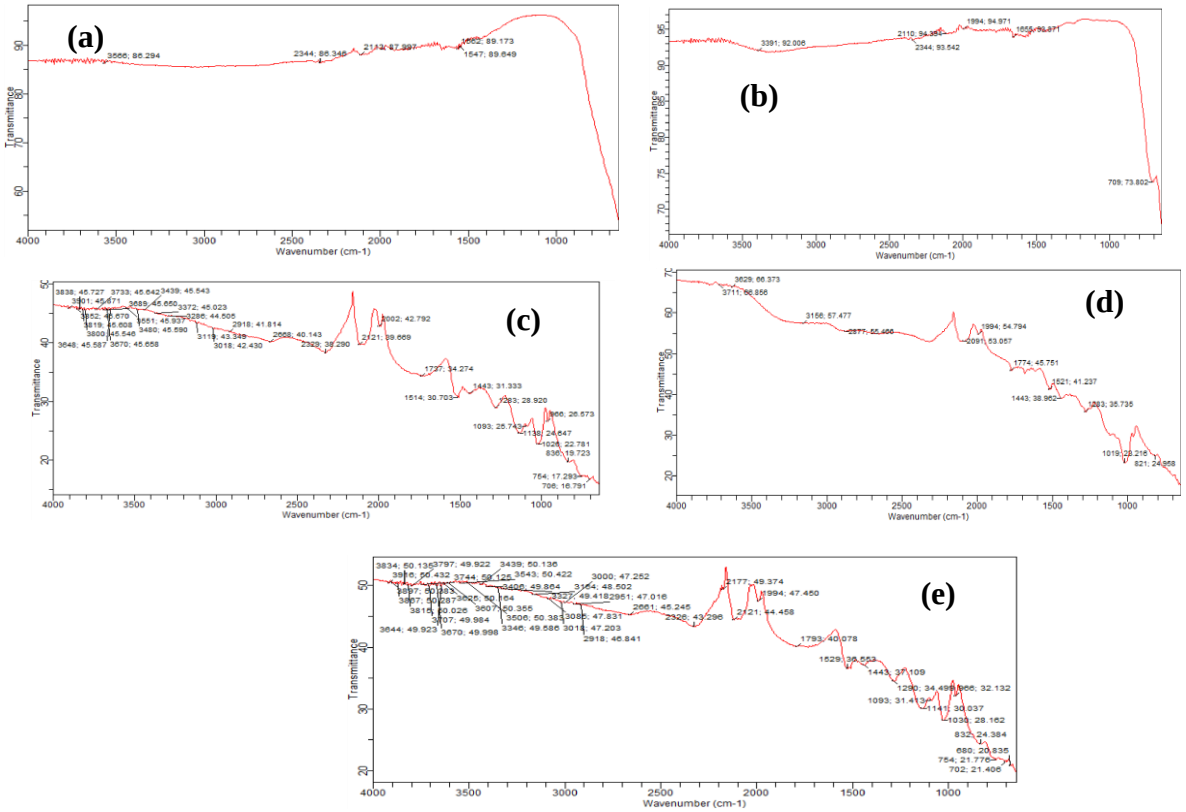

Figure 2. FTIR spectra of (a) TiO_2 NPs, (b) Zn doped TiO_2 NPs, (c) Polypyrrole, (d) PPy/TiO_2 NCs and (e) PPy/Zn-doped TiO_2 NCs

Fig. 2a depicts the FT-IR spectrum of TiO_2 NPs prepared by sol-gel method and heated at 500 ˚C for 5 hrs. The absorption band observed at 3365 cm^{-1} in the TiO_2 NPs spectrum is due to the O-H stretching vibration frequency and also signals a strong hydrogen-bonding between OH and the surface of titanium dioxide (TiO_2). The characteristic peak at 1655 cm^{-1} is assigned to the H-O-H bending vibration mode of the observed water molecule(s) as well as Ti-OH (Shen et al., 2011). From Fig. 2b, the characteristic peaks at 3566 cm^{-1} and 1622 cm^{-1} in Fig. 2 shifts to a lower wavelength region of 3391 and 1655 cm^{-1}. This could be due to introduction of 3 wt % of Zn in the Zn-TiO_2 nano particle. Fig. 2c shows the FTIR spectra of PPy. In the PPy spectrum, the bands between 1529 and 1443 cm^{-1} are due to the major vibrations of the pyrrole rings, which correspond to the asymmetric and

symmetric ring-stretching modes of PPy (Jiang et al., 2009). The absorption peak at 3439 cm^{-1} is due to the N-H stretching, the characteristic peak observed between 1290 and 1141 cm^{-1} are attributed to the C-N stretching vibration and the in-plane deformation vibration of NH^{+} and band at 1030 cm^{-1} belongs to the C-H and N-H in-plane deformation vibrations. As shown in Fig. 2d and 2e all the characteristics absorptions shifted to lower wavelengths which could be due to the introduction of TiO_2 and Zn/TiO_2 nanoparticles respectively.

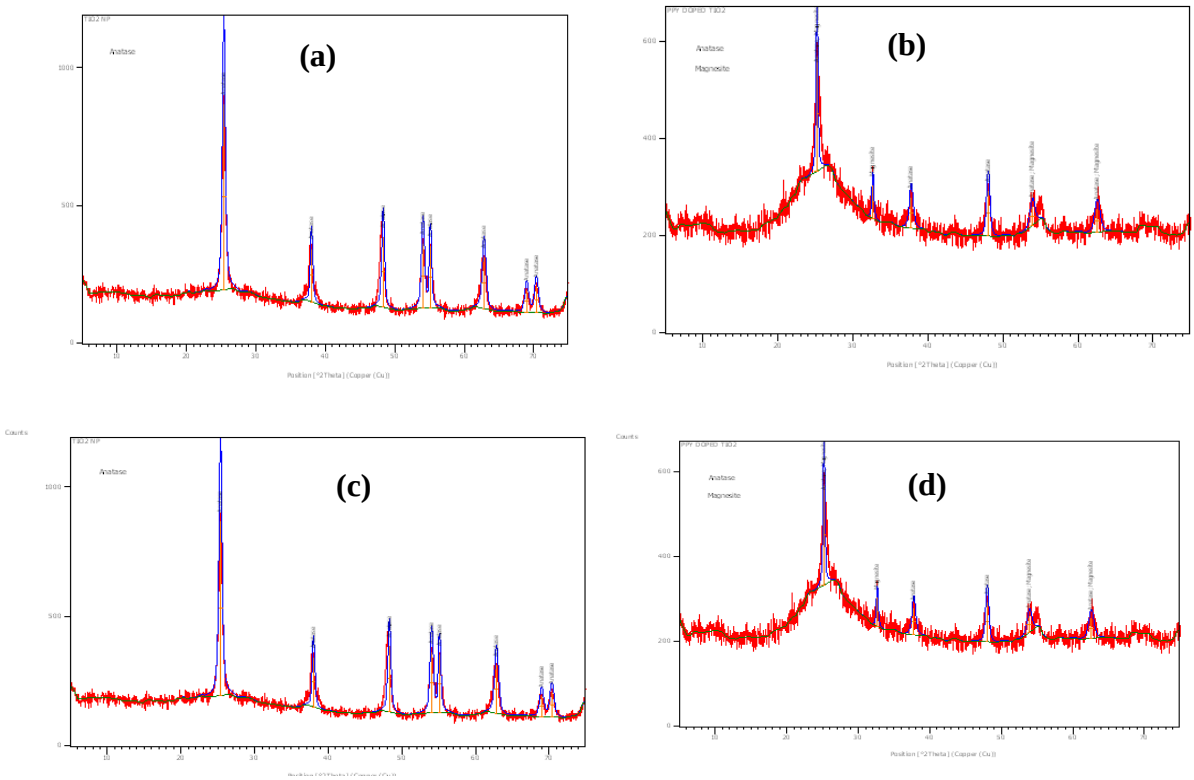

Fig. 3. XRD pattern of (a) TiO_2 NPs, (b) PPy/TiO_2 NCs, (c) Zn/TiO_2 NPs and (d) PPy/Zn/TiO_2 NCs

The XRD patterns of pure TiO_2 NPs, Zn/TiO_2 NPs, PPy doped TiO_2 and PPy doped Zn/TiO_2NCs are shown in Fig. 3 a-d. From the XRD diffraction patterns, it is observed that both the TiO_2 NPs (Fig. 3a) and Zn/TiO_2 NPs (Fig. 3b) are in anatase phase. Also, it is obvious that the XRD pattern of Zn/TiO_2 NPs (Fig. 3c) display similar XRD pattern with the TiO_2 NPs, i.e., at 3 % of zinc doping, the XRD diffraction peaks do not show any zinc phase (Karthik et al., 2010). This suggest that the zinc ions are dispersed uniformly onto the TiO_2 where the presence of zinc does not influence the growth of new crystal arrangements of TiO_2. However, the average diffraction peaks intensity of Zn/TiO_2 NPs were slightly broadened compared to the bare TiO_2 NPs. This is as a result of decrease in the crystallite size of TiO_2 in the presence of zinc doping (Mugundan et al., 2015). The average crystallite size were calculated from the (FWHM) of the XRD diffraction peaks using the Scherrer formula (Sookhakian et al., 2014).

$$D = \frac{k\lambda}{\beta cos\theta} \quad \text{.....(2)}$$

Where the parameter D is the average crystallite size of the nanoparticles, K the shape factor, which is 0.94; λ is the X-ray wavelength, β is the FWHM of the XRD diffraction pattern expressed in radian and θ is the angle of diffraction. The crystallite sizes of the nanoparticles calculated from Scherrer equation are 18.87 nm and 16.12 nm for TiO_2 NPs and Zn/TiO_2 NPs respectively. In this case Zn doping is further evidenced by the EDX charts. Furthermore, it is observed that all the prominent peaks in TiO_2 NPs and Zn doped TiO_2 NPs have appeared in the XRD patterns of PPy doped TiO_2 NCs (Fig. 3c) and PPy doped Zn/TiO_2 NCs (Fig. 3d) respectively. Figs. 4a and 4b give the EDX chart of TiO_2 and Zn-doped TiO_2 NPs respectively. The Ti and Zn peaks are detected at 4.5 keV and 1.0 keV respectively. The result confirmed the presence of Zn in the TiO_2 NPs due to the decreased in the intensity of Ti peak and appearance of Zn peak. This means some Ti atoms are substituted by Zn atoms.

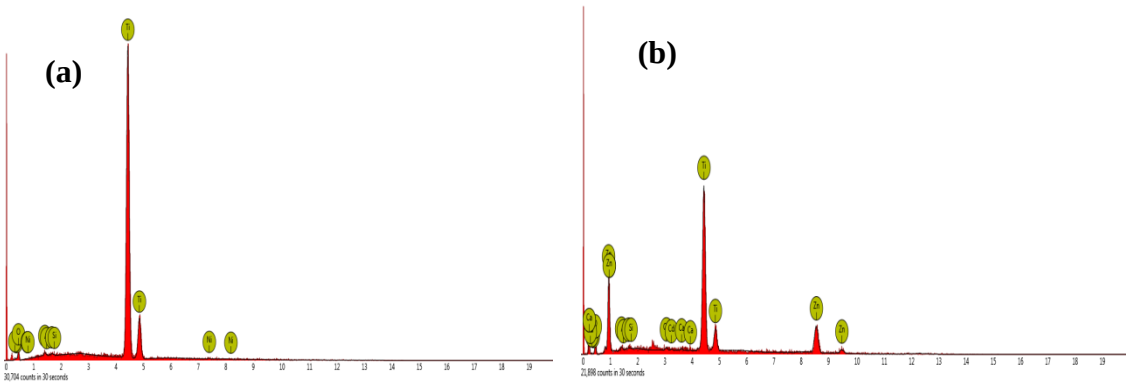

Fig. 4: Energy dispersive x-ray spectroscopy of (a) TiO_2 NPs and (b) Zn-doped TiO_2 NPs

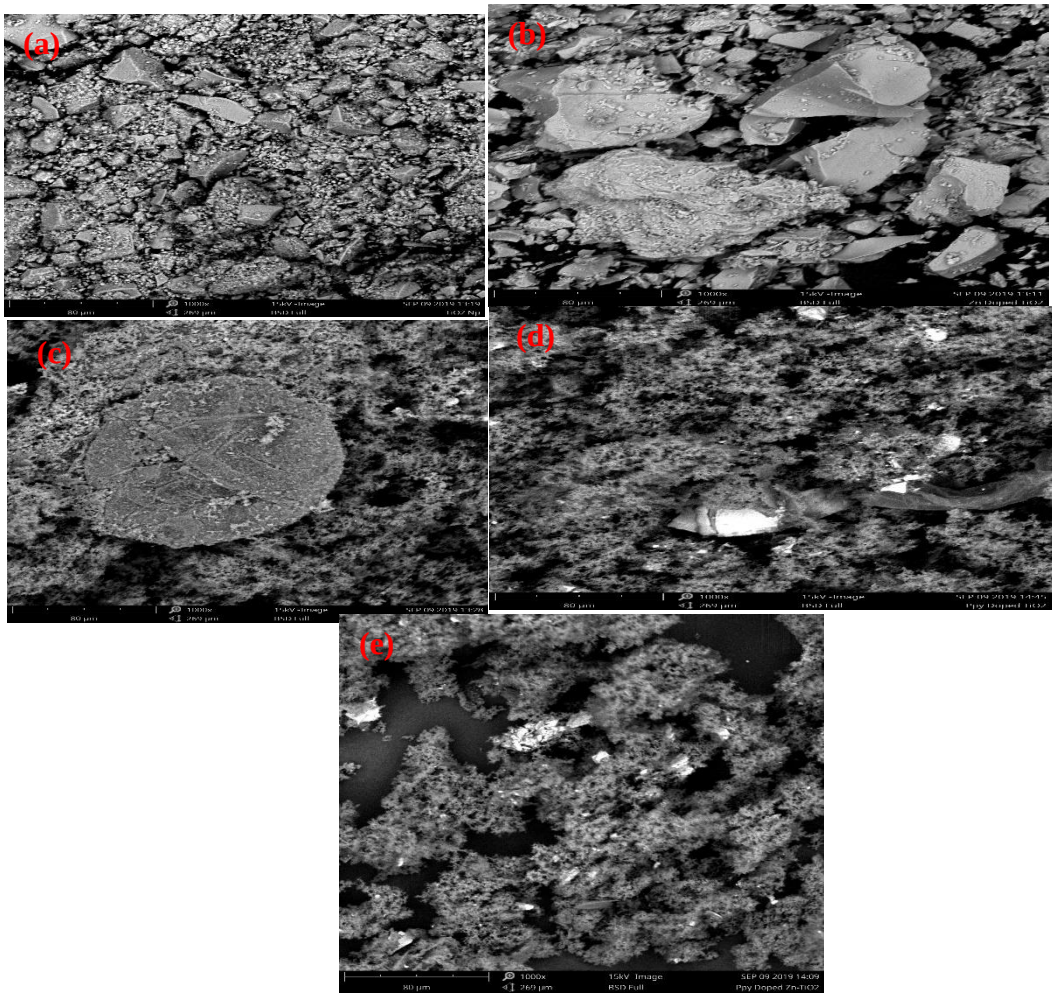

Fig. 5: SEM micrographs of (a) TiO_2 NPs, (b) Zn-doped TiO_2, (c) PPy, (d) PPy/TiO_2 and (e) PPy/Zn-doped TiO_2 NCs at a magnification of X1000.

Fig. 5a and 5b illustrate SEM images of TiO_2 and Zn-doped TiO_2nano particles respectively prepared by sol-gel method, the SEM indicates that TiO_2 and Zn/TiO_2 have tetragonal shape with cubic symmetry. The morphology of polypyrrole and the nanoparticles incorporated polypyrrole synthesized by in-situ chemical polymerization are shown in Fig. 5c and Fig. 5d. The micrograph of polypyrrole reveals the presence of globular particles. In Fig. 5a and 5b the SEM indicates that TiO_2 and Zn-doped TiO_2 nanoparticles have a nucleus effect and cause a homogenous PPy core-shell morphology leading to the coverage of TiO_2 and Zn-doped TiO_2 nanoparticles by PPy deposit (Fig. 5e). The result also showed that with the presence of nanoparticle in the PPy matrix, the PPy particles became more compacted (Hanaor et al., 2011).

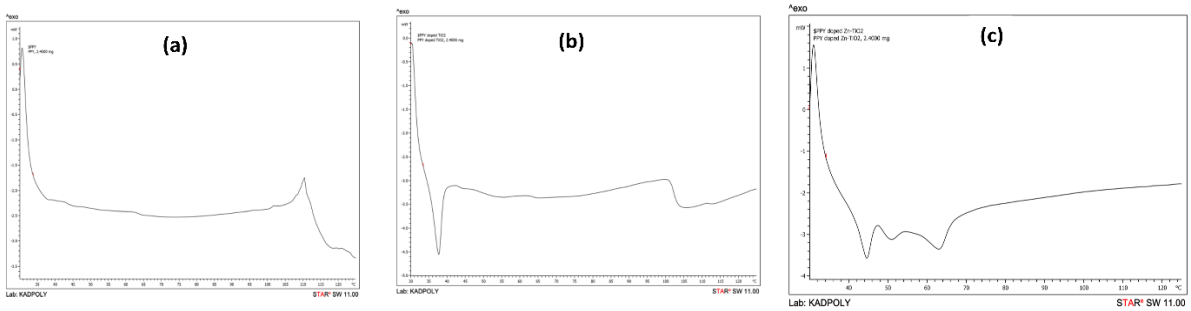

Fig. 6: DSC thermograph of (a) PPy, (b) PPy/TiO_2 NCs and (c) PPy/Zn-doped TiO_2 NCs

Table 1: Thermal properties of the polymer and polymer nanocomposites

Sample name	(T_g)	(T_c)	(T_m)	% crystallinity
Polypyrrole (PPy)	27.63 ^{0}C	-	110 ^{0}C	-
PPy/TiO_2	29.83 ^{0}C	37.77 ^{0}C	-	19.28 %
PPy/Zn-doped TiO_2	31.29 ^{0}C	44.57 ^{0}C	-	32.51 %

Fig. 6 shows the DSC thermograph for PPy (a), PPy/TiO_2 (b) and PPy/Zn-doped TiO_2 (c) obtained at a heating rate of 10 ˚C min^{-1}. From the beginning of the heating, there observed a significant endothermic baseline change which indicates heat absorption by the samples and corresponds to the glass transition temperature (T_g). for the samples. From Fig. 6a pure Polypyrrole sample is found to have an onset glass transition temperature (T_g) at 27.63 ˚C and an endothermic peak at 110 ˚C which correspond to its melting temperature (T_m). As shown in Fig. 6b, the PPy/TiO_2 NC shows glass transition temperature (T_g) at 29.83 °C and an exothermic peak at 37.77 ˚C which is due to cold crystallization process of the polymer. Moreover, from Fig. 6c, the DSC thermograph of PPy/ Zn-doped TiO_2 NC shows a T_g at 31.29 ˚C and a large exothermic peaks with one at 44.57 ˚C followed by two others at 51 ˚C and 63 ˚C. This indicates an increase in the crystallization temperature of the nanocomposite. This increase in the crystallization temperature of the nano composite can be attributed to the doping of the nanoparticles into the matrix of the poly pyrrole polymer leading to the formation of a compound with melting point considerably higher than the un-doped Polypyrrole (Sedaghat, 2014). Furthermore, from the DSC data the percentage crystallinity of the PPy/TiO_2 and that of PPy/ Zn-doped TiO_2 were found to be 19.28 % and 32.51 % respectively. Thus it might be concluded that doping of nanoparticles onto Polypyrrole causes an improvement in its thermal stability (Ladan et al., 2017).

CORROSION STUDIES

Corrosion Current Measurement using Corrosion Kit

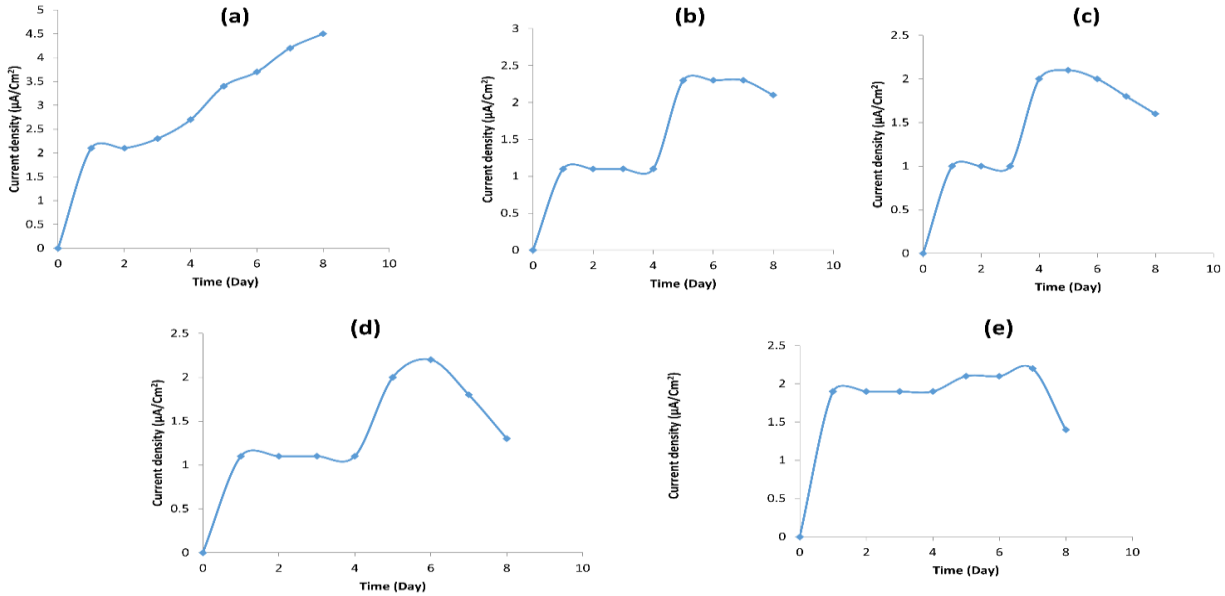

Figure 7. Corrosion current density vs elapsed time for bare mild steel (a), mild steel with epoxy resin coating (b), mild steel with PPy/epoxy coating (c), mild steel with PPy/TiO_2/epoxy coating (d) and mild steel with PPy/Zn-doped TiO_2/epoxy coating (e) in 3.5% NaCl solution

Table 2: corrosion rate parameters using Armfield corrosion kit in 3.5% NaCl solution

S/N	Sample name	corrosion current ($\mu A/Cm^2$)	Corrosion rate (mm/yr)	% efficiency (%)
1.	Blank mild steel 4.9	0.830	0	
2	Blank epoxy coated Mild steel	2.1	0.358	57.14
3	Ppy/epoxy coated mild Steel	1.8	0.248	63.27
4.	Ppy/TiO_2/epoxy Coated mild steel	1.4	0.193	71.43
5.	Ppy/zn-doped TiO_2/epoxy Coated mild steel	1.2	0.156	75.51

Figure 7a shows the relationship between the corrosion current density and immersion time of bare mild steel in 3.5% NaCl, right from the beginning (1st day) the corrosion current density was high which keeps increasing up to the eighth day. This could possibly be as a result of continuous corrosion process taking place in the electrolyte between the surface of the mild steel and the corrosive medium since there is no barrier between the surface of the mild steel and the corrosive species. From Fig. 7b, c, d and e, which corresponds to the mild steel coated with epoxy alone, mild steel coated with Ppy/epoxy blend, mild steel coated with Ppy/TiO_2/epoxy and Ppy/Zn-doped TiO_2/epoxy blend respectively, the corrosion current density remained steady up to day four which then starts increasing from day five and then later starts decreasing up to day eight. The possible reason for this increase could be as a result of barrier between the steel surface and the electrolyte as well as formation of stable passive oxide layers such as α-Fe_3O_4, α-Fe_2O_3 and β-Fe_2O_3 at the polymer-metal interface (Lenz et al 2003). Similarly the tremendous decrease in the corrosion current density observed by Ppy/Zn doped TiO_2/epoxy coating could be as a result of the fact that the Ppy/Zn doped TiO_2 nanocomposite has very large surface area (confirmed by XRD) which in turn makes it's interaction with the mild steel surface stronger.

Moreover, Table 2 shows the values of corrosion current density of the mild steel samples after day eight. The result revealed that Ppy-Zn doped TiO_2 coated sample has minimal corrosion current density compared to others after the same period whereas mild steel sample without coating shows maximum corrosion current density.

Corrosion rate (C.R) in mm/year have also been calculated using the formula shown in equation 3.

$$\boldsymbol{Corrosionrate(mm/yr)} = \frac{K1 \times Icorr \times EW}{\rho} \quad \text{.....(3)}$$

(mm/yr) = millimeter per year, K_1; constant = $3.27*10^{-3}$ mm g/μA cm yr, I_{corr} = current density in micro ampere per centimetre square (μA. cm^{-2}), EW= equivalent weight of metal, ρ = density of metal.

From the results, it was observed that the corrosion rate was highest for the uncoated mild steel in 3.5 % NaCl medium. After 8 days of corrosion current measurement, the C.R value of the uncoated mild steel was found to be 0.830 mm/year. Epoxy and Ppy coated samples showed C.R. values of 0.358 mm/year and 0.248 mm/year respectively. While in the case of Ppy-Zn doped TiO_2 coated sample at 10 % loading, C.R. value reduced to 0.156 mm/year.

The corrosion protection efficiency (% P.E.) of the coatings were also determined from the measured I_{corr} (corrosion current densities with blank mild steel electrode ($I_o$corr) without coatings and corrosion current densities with a mild steel electrode coated with polymer coated ($I_c$corr) values by using the relationship represented by equation (4).

$$P.E(\%) = \frac{IoCorr - IcCorr}{IoCorr} \times 100 \quad \text{.....(4)}$$

From the result in Table 2, the protection efficiency of blank epoxy coating was found to be only 57.14 %, while that of PPy, PPy doped TiO_2-based coatings was 63.27 % and 71,43 % respectively. In the case of PPy doped Zn/TiO_2-based coatings, highest protection efficiency of 75.15 % was recorded. The superior corrosion protection ability of the coating could be due to the increased surface area of the PPy doped Zn/TiO_2 which can increase its ability to interact with the ions liberated during the corrosion reaction of steel in the presence of NaCl (Mahmoudian et al., 2011).

CONCLUSION

Polypyrrole was synthesized in the presence of nanoparticles which results in the decrease of the size of the polypyrrole there by increasing its surface area of contact which interacts well with the steel surface.

The corrosion protection of polypyrrole increases with the increase in polypyrrole dispersion in the reaction medium. Furthermore, the protection efficiency of the coating prepared from PPy/Zn-doped TiO_2 and PPy/TiO_2 were found to be 75.51 % and 71.43 % respectively after 8 days of immersion of the coated mild steel in 3.5 % NaCl solution. Moreover, these results confirmed the better performance of the coatings incorporated with PPy/ Zn-doped TiO_2 compared to the coatings incorporated with PPy/TiO_2 NCs and PPy alone.

REFERENCES

Al-Sabagh A.M., El-Dean M.E., Hussein M.A. and Farouq N.A. (2016) polypyrrole/shells nanocomposite: preparation, characterization and application in BTX adsorption. *International journal of engineering science and computing* Vol. 6 no 10

Bai X., Tran T. H., Yu D., Vimalanandan A., Hu, X. and Rohwerder M. (2015) Novel conducting polymer based composite coatings for corrosion protection of zinc. *Corrosion Science*. 95, 110-116.

Deyab M. A., and Keera S. T. (2014) Effect of nano-TiO_2 particles size on the corrosion resistance of alkyd coating. *Material Chemistry and Physics*. 146, 406-411.

Hanaor D. A. H., and Sorrel C. C (2011) review of anatase to rutile transformation. *Journal of material science* 46, 855-874

Hsieh Y. P., Hofmann M., Chang K. W., Jhu J. G., Li Y. Y., Chen K. Y., Yang C. C., Chang W. S. And Chen L. C. (2013) Complete corrosion inhibition through graphene defect passivation, *ACS Nano* 8, 443-448.

Jiang J., Ai L., and Li L (2009) multi functionalpolypyrrole/strontium hexaferrite composite microspheres: preparation characterization and properties. *Journal of physics chemistry.* 113, 1376-1380.

Kamaraj K., Karpakam V., Sathiyanarayanan S. and Venkatachari G. (2010) Electro-synthesis of poly (aniline-co-m-amino benzoic acid) for corrosion protection of steel. *Material Chemistry and Physics* 122, 123-128.

Karthik K., Pandian S. K., Kumar K.S. and Jaya N.V. (2010) influence of dopant level on structural, optical and magnetic properties of Co-doped anatase TiO_2 nanoparticles. Applied surface science 256, 4757-4760.

Ladan M., Basirun W. J., Kazi S.N. and Abdurrahman F. (2017) corrosion protection of AISI 1018 steel using co-doped TiO_2/polypyrrole nanocomposites in 3.5% NaCl solution. *Material chemistry and physics* 192, 361-373

Lei Y., Ohtsuka T. And Sheng N. (2015) Corrosion protection of copper by polypyrrole film studied by electrochemical impedance spectroscopy and the electrochemical quartz microbalance. *Applied Surface Science.* 357, 1122-1132.

Lenz D.M., Delamar M. And Ferreira C. A. (2003) Application of polypyrrole/TiO_2 composite films as corrosion protection of mild steel, *Journal of electro-analytical chemistry* 540, 35-44.

Mahmoudian M., Alias Y., Basirun W. and Ebadi M. (2013) Effects of different polypyrrole/TiO_2nanocomposite morphologies in polyvinyl butyral coatings for preventing the corrosion of mild steel. *Applied Surface Science.* 268, 302-311.

Mahmoudian M., Basirun M., Alias Y. And Ebadi M. (2011) synthesis and characterization of polypyrrole/Sn-doped TiO_2nanocomposites as protective pigment *Applied surface science* 257, 8317-8325

Mugundan S., Rajamannan B., Viruthagiri G., Shanmugam N., Gobi R., and Praveen P. (2015) Synthesis and characterization of undoped and cobalt-doped TiO_2 nanoparticles via sol gel technique, *Applied Nanoscience.* 5, 449-456.

Olad A. and Rasouli H. (2010) Enhanced corrosion protective coating based on conducting poly aniline/zinc nanocomposit. *Jounal of applied polymer sience* 115, 2221-2227.

Shen J., Yan B., Shi M., Ma H., Li M. And Ye M (2011) one step hydrothermal synthesis of TiO_2-reduced grapheme oxide sheets. *Journal of material chemistry.* 21, 3415-3421.

Sheng X., Cai W., Zhong L., Xie D., and Zhange X. (2016) synthesis of functionalized graphene/poly aniline nano composites with effective synergistic reinforcement on anti corrosion. *Industrial and engineering chemistry Research* 55, 8576-8585.

Singh B. P., Jena B. K., Bhattacharjee S. and Besra L. (2013) Development of oxidation and corrosion resistance hydrophobic graphene oxide-polymer composite coating on copper. *Surface Coating Technology* 232, 475-481.

Sookhakian M., Amin Y., Basirun W., Tajabadi N., and Kamarulzaman N (2014) synthesis, structural and optical properties of type-II ZnO-ZnS core-shell nanostructure 142, 244-252.

Thompson N. G., Yunovich M. and Dunmire D. (2007) Cost of corrosion and corrosion maintenance strategies, *Corrosion Review* 25, 247-262.

Wei H., Wang Y., Guo, J., Shen N. Z., Jiang D., Zhang X., Yan X., Zhu J., Wang Q. And Shao L. (2015) Advanced micro/nanocapsules for self-healing smart anticorrosion Coatings. *Journal of Material Chemistry.* 3, 469-480.

Yuan R., Wu S., Wang B., Liu Z., Mu L., Ji T., Chen L., Liu B., Wang H. and Zhu J. (2016) Superamphiphobicity and electro-activity enabled dual physical/chemical protections in novel anticorrosive nanocomposite coatings. *Polymer* 85, 37-46.